Silicon (2022) 14:11453–11462
https://doi.org/10.1007/s12633-022-01865-7

ORIGINAL PAPER

Sensitivity Enhancement of Dual Gate FET Based Biosensor Using Modulated Dielectric for Covid Detection

Saurabh Kumar[1] · R.K. Chauhan[1] · Manish Kumar[1]

Received: 2 December 2021 / Accepted: 31 March 2022 / Published online: 12 April 2022

Abstract

This paper presents a dual gate dielectric modulated FET (DGDMFET) biosensor with enhanced sensitivity for covid detection. In earlier literature, the biosensors are operated using the surface interaction with the virus biomolecules that are reflected through a channel or gate. The downside of these types of sensors has limited sensitivity. In this paper, we have considered that the change in the dielectric constant due to virus proteins results in a significant shift in the threshold voltage of FET. Enhancement of sensitivity is done by using the novel dual metal gate arrangement with different work functions (higher at the source end and lower at the drain end) and the chromic oxide (Cr_2O_3) layer, which is carved out vertically to form nanogap. At the same time, interface charge density is maintained nearly equal to 1.0×10^{11} cm^{-2} at the Si-SiO_2 layer. To demonstrate the proposed biosensor, electrical parameters (electron concentration, surface potential, energy band distribution, and electric field) and the absolute percentage sensitivity of threshold voltage, subthreshold slope, ON current, and transconductance are evaluated and compared with related literature. The ATLAS device simulator is used for the simulation of the proposed device.

Keywords Biosensor · Dielectric modulation · Nanogap · Dual gate

1 Introduction

Coronavirus disease 2019 (COVID-19) was declared a pandemic on March 13, 2020. In December 2019, a COVID-19 outbreak was reported; it caused the world's economic recession and millions of deaths [1, 2]. In the year 2002–2003, severe acute respiratory syndrome coronavirus (SARS-CoV) [3]. In 2012 the Middle East Respiratory Syndrome coronavirus (MERS-CoV) [4]. The recent one is the new type of SARS, namely SARS-COV-2 is also caused by coronavirus only [5]. This virus is transmitted through touching a contaminated surface that contains a virus, coming in direct contact with the infected person's respiratory droplet (generated at the time of coughing and sneezing) [6]. The SARS-CoV-2 has been found in feces samples, so virus transmission can occur through an unhygienic and unhealthy lifestyle. It has been observed that in many cases, the virus is transferred through asymptomatic patients [7, 8]. The complication due to COVID-19 is coagulopathy, neurologic complications, post-acute COVID-19 syndrome (PACS). Increased fibrinogen levels and D-dimer characterize coagulopathy, which causes venous thromboembolism (VTE), thromboprophylaxis. In neurologic complications, reported complications include stroke, encephalitis, meningitis, myalgia/myositis, Guillain-barre syndrome, acute disseminated encephalomyelitis (ADEM), acute hemorrhagic necrotizing encephalopathy, and ataxias [9]. According to WHO, on august 6, 2021the reported death due to COVID-19 was 4,265,903, which is enough to horrify the world. No specific drugs or vaccines against COVID-19 have been available till now. Therefore, social distancing, personal hygiene, isolation of infected people, mass screening of infected ones (with or without symptoms), and timely treatment have shown positive responses to break the chain of community transmission [10]. Along with the pathological information, the structure of SARS-CoV-2 is also needed to design the biosensors to detect COVID-19. The structure of the SARS-CoV-2 virus contains a circular shape

✉ Saurabh Kumar
saurabh.k2u@gmail.com

R.K. Chauhan
rkchauhan27@gmail.com

Manish Kumar
er.manish.k@gmail.com

[1] Department of Electronics & Communication Engineering, M.M.M. University of Technology, Gorakhpur, India

of a thin membrane, spike proteins, and envelope; this image is issued by the center for disease control and prevention (CDC), USA [11], as shown in Fig. 1.

2 Recent Detection Methods of Virus

There are three different diagnosis processes involved in the detection of SARS-CoV-2, including (1) RNA detection using real-time reverse transcription-polymerase chain reaction (RT-PCR) assay [12], (2) fully automatic chemiluminescence method, lateral flow assays, enzyme-linked immunosorbent assay (ELISA) for the determination of antibodies [13], (3) CT scan of the chest along with clinical indications [14]. Nevertheless, a chest CT scan has many drawbacks, like it does not differentiate whether the infection is caused by SARS CoV-2 or by any other virus. It requires a well-trained radiologist to analyze the CT scan images, it is costly enough for poor people, and also it is only limited to big hospitals. ELISA is the conventional method to detect the virus. The associated antibodies in the blood serum of the patients are observed to detect the virus, not the virus directly is detected. In the ELISA test, the presence of IgG (immunoglobulin G) antibodies in human serum indicates that the person was infected with the SARS CoV-2 virus in the past and has now developed an appropriate immune response to combat the virus in their system. The detection of immunoglobulin M (IgM) antibodies in human blood serum indicate that the person is recently infected with the virus. ELISA test for SARS CoV-2 is performed by fixing the S-protein of the virus on the testing plate, and the patient's blood sample (mainly the serum) is occupied over it. Suppose the antibodies are present in the patient's blood sample-like IgG or IgM. In that case, it attaches with the spike protein of the virus immobile on the plate of the testing kit, the linkage of the patient's antibody and HRB (which is lab manufactured having red color antibodies) make substrate colorless. It indicates that the patients have been infected with the SARS CoV-2 virus [15, 16].

Advanced and rapid testing kits follow the RT-PCR testing method; RNA is converted into complementary DNA first. Then, the DNA signal is amplified by using a real-time polymerase chain reaction. In RT-PCR, the probe strand, which contains two dyes: a quencher and a reporter, binds to a specific target sequence to virus SARS-CoV-2, placed between the forward and reverse primer. During the PCR cycle extension phase, the bound probe is degraded by the polymerase, which causes the separation of reporter dye from the quencher dye, due to which the fluorescent signal is increased. At each amplification cycle, the fluorescent intensity is monitored; as more copies of DNA are produced, the fluorescence signal increases, and when it crosses a certain threshold set above an expected background level. The result is positive, and if the fluorescence threshold is not reached, the result is then negative. The RT-PCR test is time-consuming and requires a trained technician [17]. So, to overcome these disadvantages, new devices and diagnostic tests for virus detection in clinical samples that are faster, more precise and reliable, more accessible, and cost-efficient than existing ones are needed.

Ion sensitive field-effect transistors (ISFET) and microelectronic device sensors based on thin-film transistors have been a low-cost alternative to traditional chemical sensors since the early 1970s. However, lack of parasitic sensitivity to light and temperature, instability of sensor parameters and prominent space on-chip, etc. Make the researchers invent new nanodevices for sensing applications [18]. FET-based biosensors known for their widespread sensing capability revolutionize the health industry and can also be used to maintain our ecosystem. Much research has been made to increase the

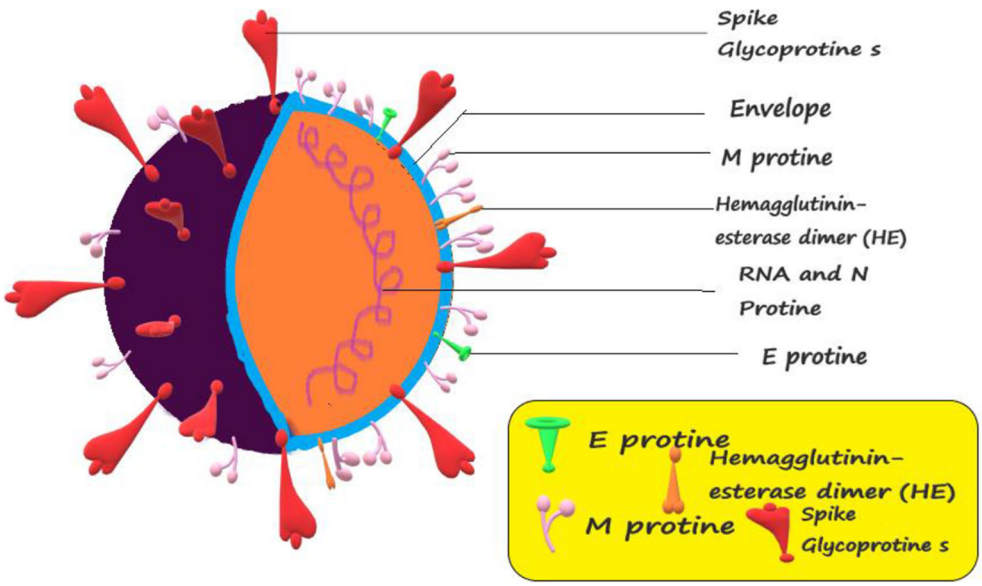

Fig. 1 Covid 19 particle structure [11]

sensitivity and decrease the power required to operate such devices [19–22]. Tunnel field-effect transistor (TFET) based biosensor achieves superior sensitivity and response time than conventional FET-based biosensor, but TFET suffers from fabrication complexity [23–25]. Silicon on Insulator (SOI) has the advantage of better gate control over the channel, low area of the source, and drain junction. The substrate's electrical insulation reduces its static and dynamic power dissipation due to lower leakage current; SOI MOSFET is the first choice for typical power applications. It can be used to operate at higher temperatures. The direct adaptation of the bulk IC design method is allowed for SOI; it requires fewer photolithography steps [26–28]. The use of chromic oxide as a gate dielectric material in field-effect transistors provides a better result as compared to other high K materials because it shows high oxidation resistance, high melting temperature, wide bandgap, and low dielectric loss. Due to its properties, it can also help to increase the sensitivity of FET-based biosensors [29].

In this manuscript, a dual gate FET-based biosensor has been proposed, which can be used to detect the virus through the dielectric constant of the Converted-DNA and Spike-protein of SARS CoV-2. We can sense the virus in two ways, the first one is S - protein recognition, and the second one is DNA protein recognition. The DNA dielectric constant ranges from 1 to 64 [30]. Spike-protein of the SARS Cov-2 virus consists of glycoprotein; in general, the spike protein of the virus is similar to proteins like 3-aminopropyltriethoxysilane (APTEs), biotin, and streptavidin, so its dielectric constant may lie somewhere between 1 to 4 [31–34]. In this paper, we have checked the sensitivity in both ways of the proposed DGDMFET.

3 Device Structure and Fabrication Process

The proposed device is a dual gate dielectric modulated field-effect transistor designed to detect SARS-CoV-2 and other viruses. It is different than conventional MOSFET because it consists of nanogap at the edge of the gate dielectric where the biomolecules are attached for detection purposes. In the traditional MOSFET, when the gate voltage is applied, it creates an electric field that affects channel potential through the gate dielectric in a silicon substrate. In the conventional MOSFET, when the channel is formed on the silicon substrate, it will start conducting, and it is known to be in an ON state. The gate voltage at which the channel is formed is known to be threshold voltage (V_{th}). In the proposed sensor device, the amount of gate voltage is insufficient to turn on the silicon channel because the electric field is not enough due to the nanogap formed, which is filled with air (dielectric constant = 1). The threshold voltage (V_{th}) value for the proposed sensor device is large as compared to conventional MOSFET because the dielectric constant of air is 1, while that of SiO2 is 3.9, so when the nanogap is formed, which is filled with air increases the V_{th} value. When the nanogap is filled with a biomolecule whose dielectric constant is more than air, the electric field is strengthened, decreasing the V_{th} value. By monitoring this change in V_{th}. The biomolecule-specific binding is electrically detected without labeling.

Figure 2 shows the proposed sensor structure and its relevant dimension. The gate length of the proposed sensor is 1um, in which the gate one and gate two lengths are 500 nm and 500 nm, respectively. Gate one is made up of gold (Au), and gate two consists of tungsten (W). The source or drain length is 250 nm, the SiO2 (oxide) thickness is 5 nm, and the Cr_2O_3 thickness is 15 nm. Both the nanogaps are of length 350 nm and thickness is 15 nm which is large enough for immobilization of biomolecules and their detection. The thickness of buried oxide is 130 nm, and its length is nearly equal to the lateral length of the device, which is 1500 nm; the width of the whole device is 1um.

Figure 3 shows the fabrication process of the proposed sensor device; for fabricating the proposed sensor device conventional complementary metal-oxide-semiconductor (CMOS) process is used. Photolithography and ion implantation after the device isolation step is used for defining the source and drain region. SiO_2, Cr_2O_3, and dual gates (Au and W) are sequentially grown and deposited using thin film. Fabrication of dual metal gates is done using the interdiffusion process of one metal on to other [35]. Silicon oxide and Cr_2O_3 form the gate dielectric of the proposed sensor device. These three layers, after deposition patterned by a photolithography process and the subsequent process of etching, lateral wet etching of Cr_2O_3 is done to form the nanogap.

4 Operation Principle

According to Kim, the threshold voltage of a conventional n-channel MOSFET is defined by Eq. (1) [30].

$$V_{th} = V_{FB} + 2\varphi_B + \frac{Q_{dCD}}{C_{OX}} - \frac{Q_{fCD}}{C_{OX}} \tag{1}$$

V_{FB} represents flat band voltage, V_{th} is the threshold voltage, φ_B is the surface-band banding, Q_{fCD} is the fixed charge density in the SiO_2 layer and Q_{dCD} is the depletion charge density. C_{OX} is the oxide capacitance of gate dielectric material which is SiO_2, in the case of conventional n-channel MOSFET?

Applying the above equation to the proposed sensor structure, we can get

$$V_{th} = V_{FB} + 2\varphi_B + \frac{Q_{dCD}}{C_{PDOX}} - \frac{Q_{fCD}}{C_{PDOX}} \tag{2}$$

Fig. 2 Proposed device structure

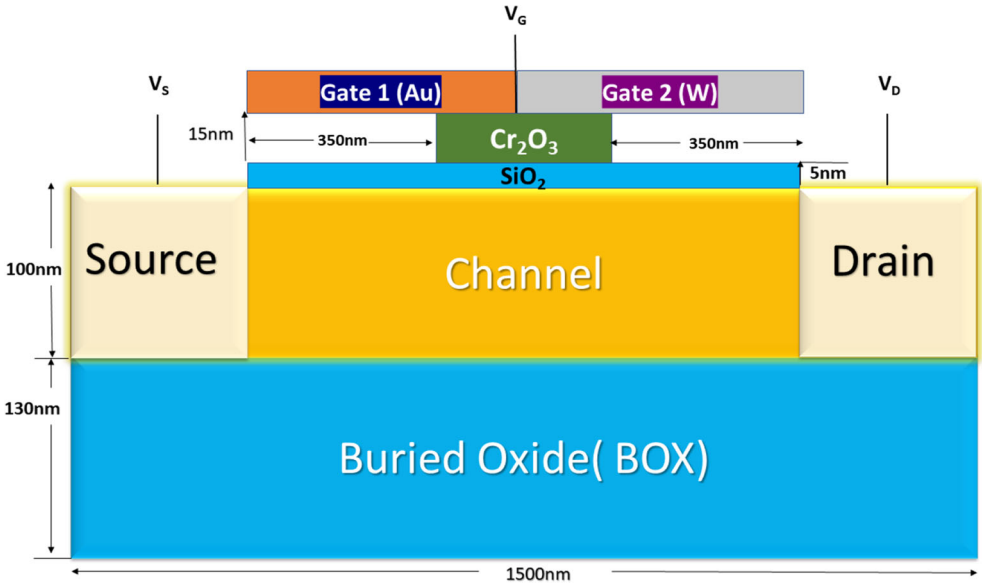

$$C_{DGDMFET} = \frac{1}{\frac{1}{C_{biomole}} + \frac{1}{C_{air}} + \frac{1}{C_{Sio_2}} + \frac{1}{\frac{1}{C_{Cr_2O_3}} + \frac{1}{C_{Sio_2}}}} \quad (3)$$

where,

$$C_{Sio_2} = \frac{K_{Sio_2}\,\epsilon_0}{T_{Sio_2}}, C_{Cr_2O_3} = \frac{K_{Cr_2O_3}\,\epsilon_0}{T_{Cr_2O_3}}, C_{air} = \frac{\epsilon_0}{T_{air}}, C_{biomole} = \frac{K_{biomole}\,\epsilon_0}{T_{biomole.}}$$

The total capacitance of the gate dielectric material is given by $C_{DGDMFET}$. Parameters mentioned in eq. (3) are $C_{biomole}$, $T_{biomole}$, $K_{biomole}$ they represent the capacitance, thickness, and dielectric constant of the biomolecule. C_{air}, T_{air} represent the capacitance and thickness of air. T_{Sio_2}, C_{Sio_2}, K_{Sio_2} represent the capacitance, thickness, and dielectric constant of silicon dioxide, i.e., SiO_2. $T_{Cr_2O_3}$, $C_{Cr_2O_3}$, $K_{Cr_2O_3}$ represent the thickness, capacitance, and dielectric constant of Cr_2O_3.

From the Eqs. (2) and (3), it can be clearly analyzed that C_{PDOX} can be altered only by the dielectric constant and charge of biomolecules. Cr_2O_3 and SiO_2 are the dielectric material apart from the nanogap region, and it can indicate that V_{th} is always lowered in Cr_2O_3 and SiO_2 region as

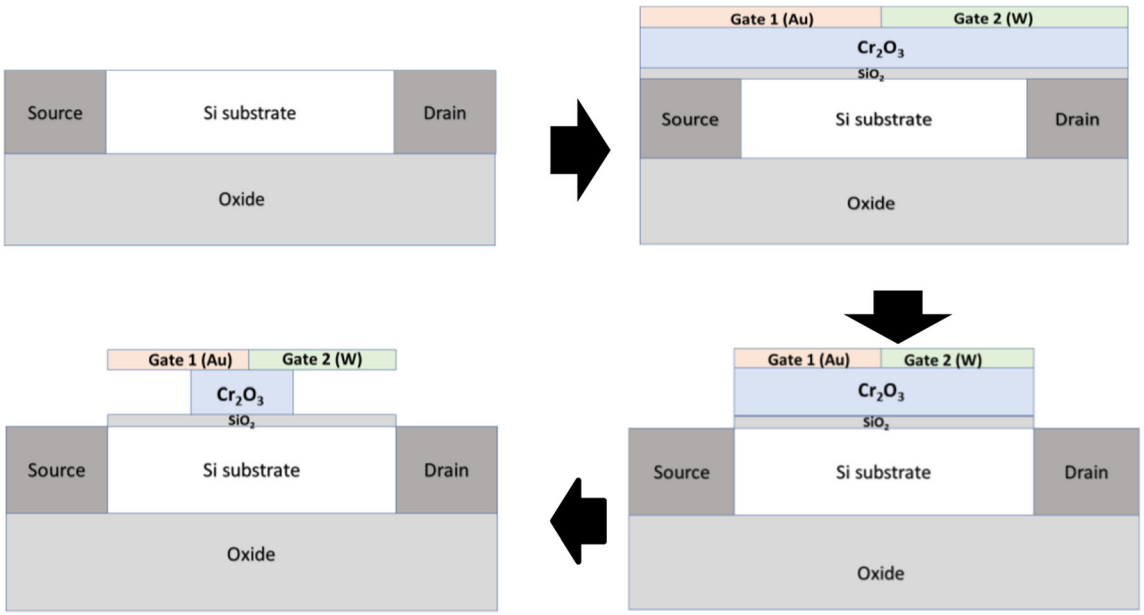

Fig. 3 Fabrication process flow of proposed biosensor

compared to air (nanogap region). Therefore, V_{th} will respond more sensitively to the change in the nanogap region dielectric constant.

According to Eqs. (2) and (3), V_{th} can be estimated when neutralized DNA is introduced in the nanogap region. V_{th} can be altered when the previously immobilized DNA in the nanogap region acts as a probe DNA and is hybridized with the target DNA. The dielectric constant of the biomolecule layer increases with the increment of the density of the biomolecule layer.

5 Simulation Methodology

The proposed sensor device is the extended form of the actual device [36] with the dual gate and Cr_2O_3 oxide layer modification. The simulation of the proposed sensor device is done using a single gate and dual-gate. In the dual-gate structure, gate one that is nothing but gold (Au) is attached to the source side, and gate two wolfram (W) is attached to the drain side. Figure 4 shows a variation of charge density at the Si-SiO_2 interface on a single gate proposed device structure. For dielectric constant (K = 2.1), the percentage V_{th} sensitivity decreases as interface charge density increase beyond 1.0×10^{11} cm^{-2} and percentage V_{th} sensitivity increases for dielectric constant (K = 4.1) with an increase in interface charge density. Therefore, the optimal value of interface charge density is chosen as 1.0×10^{11} cm^{-2} for simulation and further explanation. The percentage sensitivity is calculated using Eq. (4) adapted from [37].

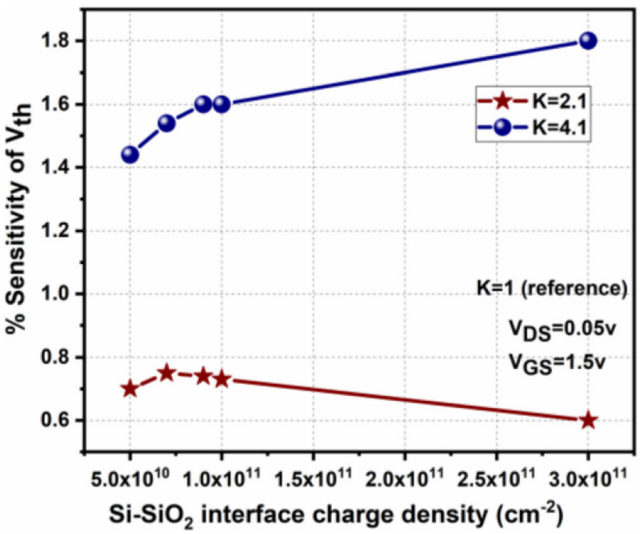

Fig. 4 Absolute percentage sensitivity variation of threshold voltage with different interface charge densities for various dielectric constant (K = 2.1, 4.1), K = 1(air) is taken as reference in the nanogap region)

6 Results and Discussion

Simulation of the proposed DGDMFET with the conceptual discussion clearly shows the significance of using a dual gate. Figure 5(a)-(e) compares the electron concentration, surface potential, energy, transconductance, and drain current between the proposed device's single gate and dual-gate structure. Figure 5(a) shows that the electron concentration is higher towards the drain side of the channel due to the lesser work function of gate 2. This rise in the electron concentration is because of work function engineering. The increase in surface carrier concentration causes an increase in the surface potential under gate two, as shown in Fig. 5(b). the influence of work function engineering and performance of the proposed sensor is further analyzed by observing the energy band diagram. In Fig. 5(c), it can be observed that under gate two, the conduction band and valence band both have a downshift that indicates a higher electron concentration in the specific region. Figure 5(d) shows that the high electron concentration under the gate2 part results in a higher drain current. The I_D versus V_{GS} curve shows that the drain current is better in the dual gate device structure than the single gate device structure. Now transconductance is also investigated of the proposed biosensor device. It indicates a better transconductance in the case of dual-gate device structure due to better drain current in the same case. From gm curve Fig. 5 (e), it can be concluded that the sensitivity for virus immobilization of the proposed device with dual gate is higher.

The impact of two metal gates, gate 1 (Au) and gate 2 (W), have been analyzed in terms of threshold voltage (V_{th}) and ON current (I_{on}). The graphs confirm the better sensitivity of dual gates in comparison to the single gate. The graph of V_{th} sensitivity indicates a significant increase in sensitivity for dual-gate, as shown in Fig. 6(a). Figure 6(b) also confirms the better sensitivity in terms of ON current. The percentage sensitivity is calculated according to Eq. (4).

6.1 Sensitivity Analysis

Some physical characteristics are investigated to show the physics and essential working of the proposed sensor device. We are going to analyze the sensitivity in two cases; in case 1, we considered the dielectric constant as 2.1 and 4.1 because the S- protein of the virus has a dielectric constant in the range between 2 to 4, and in case 2, the dielectric constant considered is in the range between 1 to 64 (DNA detection of virus). Until now, the dielectric constant of the SARS-CoV-2 virus has been unidentified, but it lies in between the range 1 to 64; that is why we are considering the same range for detection purposes.

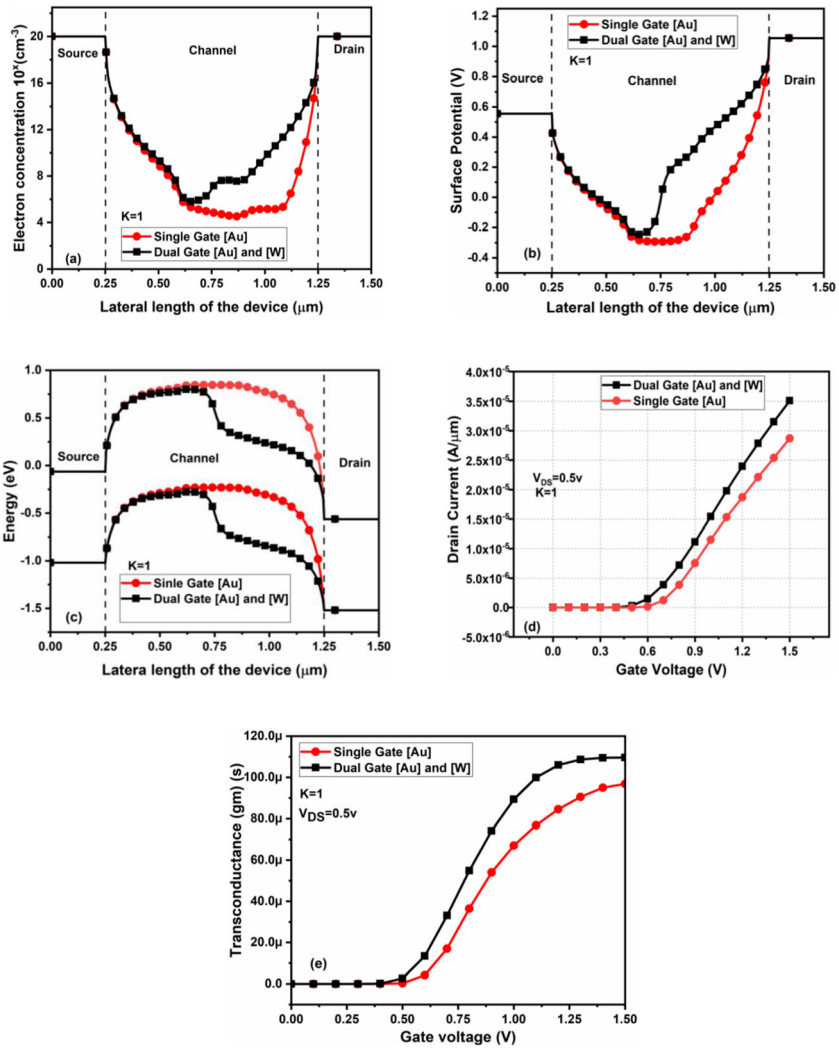

Fig. 5 Comparison between the single gate and dual gate structure of proposed biosensor in terms of (**a**) electron concentrations, (**b**) ON state surface potential distribution (**c**) Energy band distribution (EBD), along the lateral length of the device (**d**) transfer characteristics and (**e**) transconductance with gate voltage when K = 1(air) is considered inside the cavity

6.1.1 Virus Protein Having a Dielectric Constant (K = 2.1, 4.1)

Dielectric constant K = 1(air) is taken as reference for sensitivity calculation, and percentage sensitivity for various parameters is calculated as Eq. 4. [37]

$$Sensitivity = \left| \frac{D}{V_{k=1}} \right| \tag{4}$$

Where $D = \{(V_{k\ =\ 1}) - (V_{k\ =\ other\ than\ 1})\}$

Value of quantity when dielectric constant K = 1 (air) is occupied in the sensing region is denoted by $V_{k\ =\ 1}$ and $V_{k\ =}$

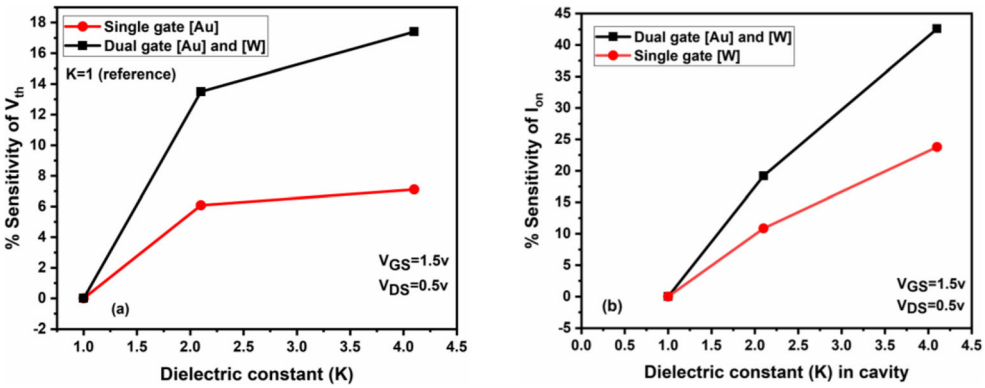

Fig. 6 The comparative plot of absolute percentage sensitivity of (**a**) V_{th} and (**b**) I_{on} for various dielectric biomolecules

other than 1 is the quantity value when dielectric constant K = 2.1 or 4.1 etc. (dielectric constant of virus protein) is filled in the sensing region. Percentage sensitivity is nothing but sensitivity multiplied by a hundred. Eq. (4) gives the absolute percentage deviation of sensor electrical parameters to air after the virus proteins are immobilized in the nanogap region.

Figure 7 represents the physical characteristics along the total device length for various K (2.1, 4.1). The 7(a) part shows variation in the valence band and conduction band for different dielectric constants; it is clearly seen from the figure that more variations of EBD is under gate 1 (having higher work function), and abrupt change is observed at the junction of the dual gate due to different work function. As the dielectric constant increases, the variation in the energy band diagram for different dielectric constant (K) shows the sensitivity for immobilized protein. The variation in the electric field can also be observed in Fig. 7(b) with various dielectric constants. Figure 7(c) and (d) show the electron concentration and surface potential variation with different dielectric constants. It is visible that the significant value of electron concentration shows better sensitivity under the cavity, and surface potential is higher under the cavity, which is below gate 2 (W), having a lower work function as compared to gate 1 (Au). Figure 7(e) is the graph between drain current and gate voltage, indicating a rise in drain current, and this variation shows sensitivity with the virus protein's dielectric constant. Figure 7(f) shows a small variation in OFF current with an increase in dielectric constant.

Figure 8 indicates the sensitivity analysis of the proposed biosensor device. Threshold sensitivity versus dielectric constant is plotted in Fig. 8(a), which indicates an increasing trend in sensitivity with the increase in dielectric constant. To decide the sensitivity of the proposed device, one of the critical parameters is the threshold voltage. In the graph, K = 1 (air) is taken as a reference, so sensitivity is zero when air is filled in the cavity. Figure 8(a) also indicates a comparative analysis

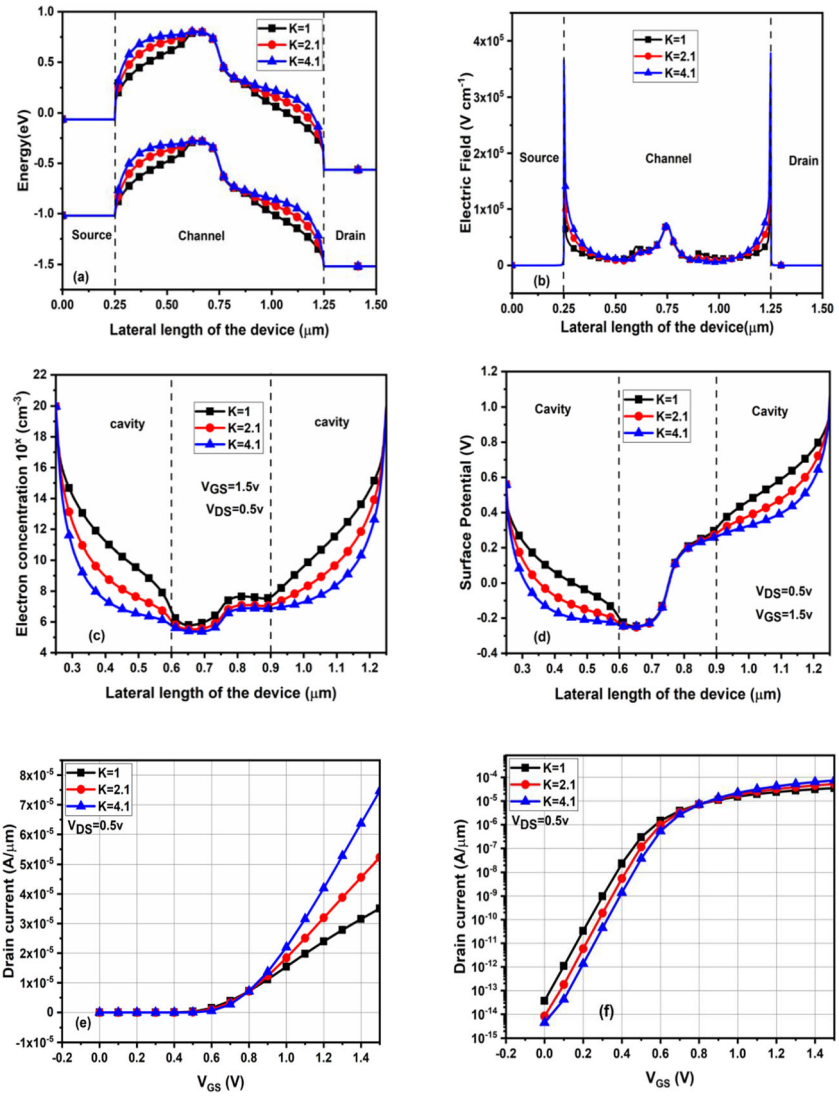

Fig. 7 Comparative plot of (**a**) EBD along device length, (**b**) electric field along device length, (**c**) electron concentration under the cavity, (**d**) surface potential distribution under the cavity, (**e**) transfer characteristics, and (**f**) OFF current variation for different dielectric biomolecules

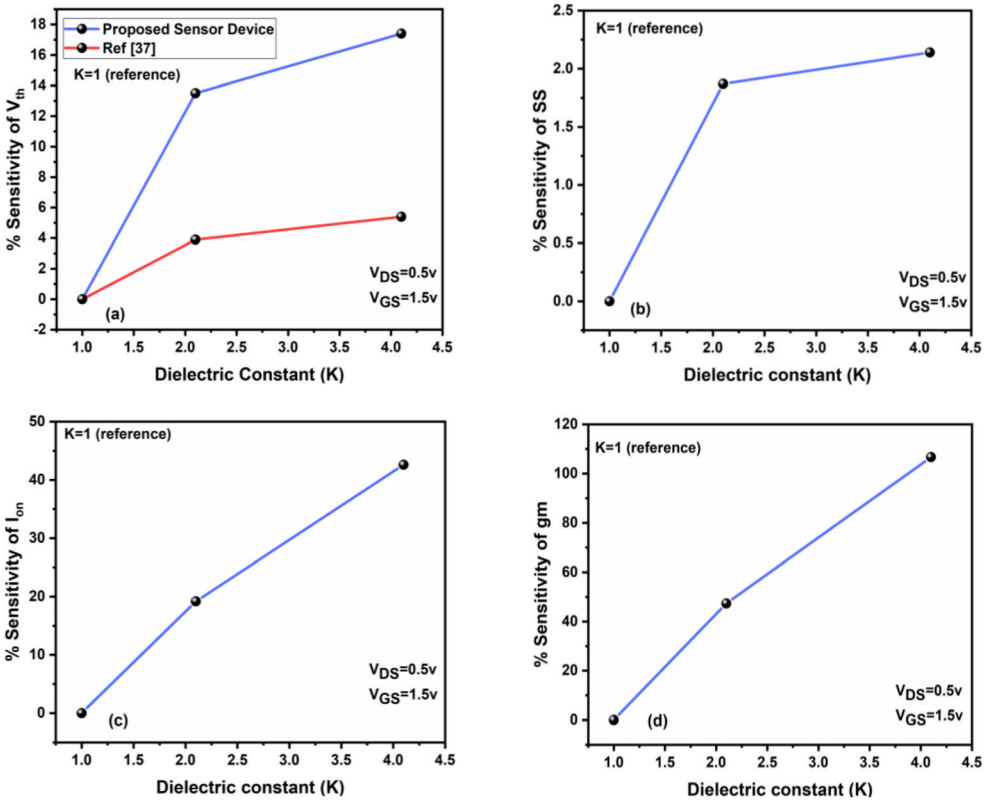

Fig. 8 (**a**) Comparison of absolute percentage sensitivity of V_{th} in between proposed sensor device and device mentioned in reference [37]. Variation in absolute percentage sensitivity of (**b**) subthreshold swing (SS), (**c**) I_{on}, and (**d**) transconductance for different virus protein dielectric constant

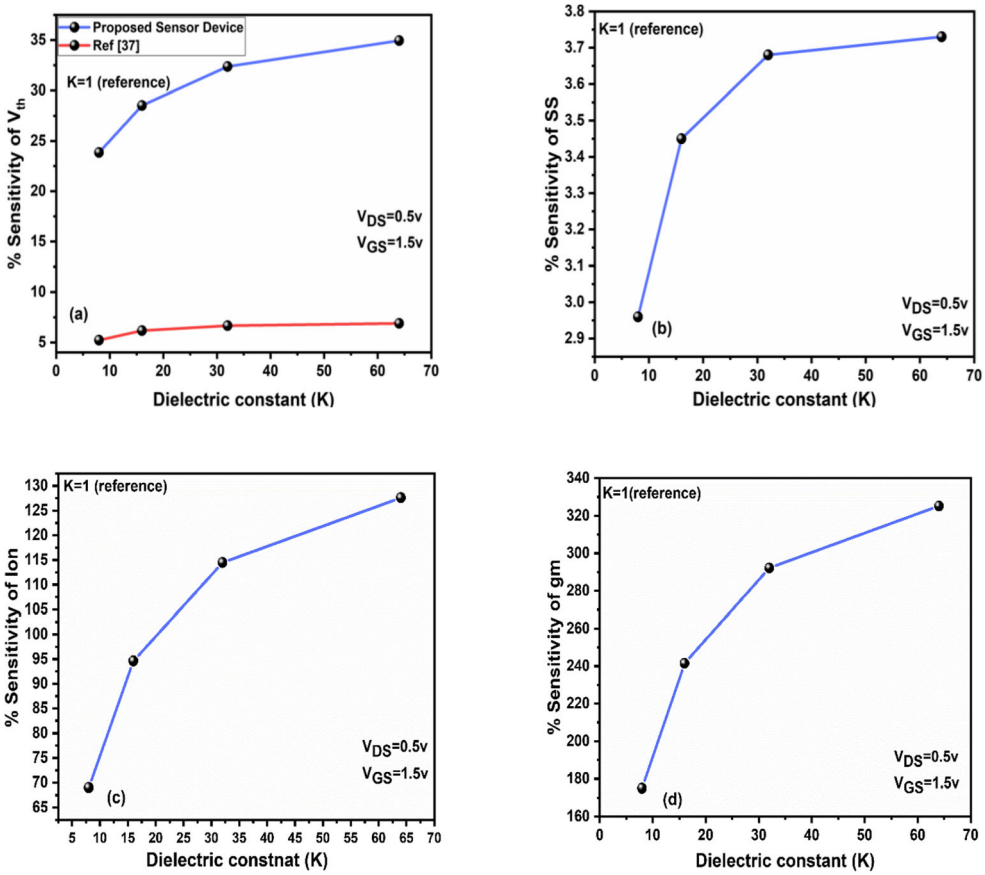

Fig. 9 (**a**) Comparison of absolute percentage sensitivity of V_{th} in between proposed sensor device and device mentioned in reference [37] with respect to DNA dielectric constant biomolecules. Variation in absolute percentage sensitivity of (**b**) SS, (**c**) I_{on}, and (**d**) transconductance for various DNA dielectric constant of the virus

between two sensor devices. One with a red color line is the device mentioned in reference [37], and the blue color line is used for the proposed sensor device. From the graph, it is clearly observed that the proposed sensor device shows significant improvement in sensitivity as compared with the reference one. Figure 8(b), (c) and (d) represent variation in sensitivity of subthreshold slope on current and transconductance with the dielectric constant of virus protein (2.1, 4.1). The use of a Dual metal gate with Cr_2O_3 improves the ON current sensitivity, which leads to a rise in gm sensitivity, as shown in Fig. 8(c) and (d)

6.1.2 Dielectric Constant of Virus in the Range from 1 to 64 (DNA Detection)

As discussed in the introduction, the second methodology used for SARS-CoV-2 virus detection is detecting through DNA; for this purpose, the DNA of the virus is converted from RNA. The SARS-CoV-2 dielectric constant is still vague, but the range of the dielectric constant is 1 to 64 [30]. The parameters are examined in terms of the DNA of the virus and found a great amount of sensitivity.

Figure 9. (a) shows a continuous increase with the DNA of virus protein; in the same figure, the proposed sensor device shows far better sensitivity than the reference biosensor device. Figure 9(b) plot of subthreshold sensitivity with DNA dielectric of virus protein shows an increasing pattern. After K = 32, the graph shows a minimal increase for higher K of the virus. An improved coupling between the channel and the gate voltage is provided by a high K value, due to which ON current sensitivity is showing an increasing trend as plotted in Fig. 9(c). RF parameter gm also indicates an increase in sensitivity with DNA dielectric of virus protein, as plotted in Fig. 9(d). The ATLAS device simulator is used for this simulation of the proposed device [38].

7 Conclusion

The sensing ability of the biosensor proposed in this paper is attained with the conclusive effect of the dual gate and use of Cr_2O_3 oxide layer by keeping the Si-SiO_2 interface charge density around 1.0×10^{11} cm^{-2}. The removal of the insulating gate layer from both the source and drain side partially creates more cavity space for biomolecules immobilization. The internal physics of the proposed biosensor is given by using various DC parameters for optimization. An investigation of the proposed biosensor with the single and dual gate in terms of DC parameters is analyzed, revealing a better result for the double gate. The proposed biosensor shows a 12% increase in threshold sensitivity for the dielectric constant of virus protein K = 4.1 as compared with the previously reported sensor [37], which discloses that the proposed biosensor has better sensitivity than the several previously reported FET biosensors. From the analysis, it can be concluded that the proposed DGDMFET biosensor will have the capability to detect various protein molecules like cancer markers, DNA, and antibodies.

Authors Contribution All authors contributed to the study's conception and design. Material preparation, data collection, and analysis were done by Saurabh Kumar, R.K.Chauhan, and Manish Kumar. The first draft of the manuscript was written by Saurabh Kumar, and all authors commented on previous versions of the manuscript. All authors read and approved the final manuscript.

Data Availability This manuscript has no associated data.

Declarations

Ethics Approval The author has followed all ethics standards

Consent to Participate Not Applicable

Consent for Publication Not Applicable

Conflict of Interest The authors have no conflicts of interest to declare that are relevant to the content of this article.

References

1. Fauci AS, Lane HC, Redfield RR (2020) Covid-19 — navigating the uncharted. N Engl J Med 382:1268–1269. https://doi.org/10.1056/NEJMe2002387
2. Santiago I (2020) Trends and innovations in biosensors for COVID-19 mass testing. ChemBioChem 21:2880–2889. https://doi.org/10.1002/cbic.202000250
3. Drosten C, Günther S, Preiser W, van der Werf S, Brodt HR, Becker S, Rabenau H, Panning M, Kolesnikova L, Fouchier RAM, Berger A, Burguière AM, Cinatl J, Eickmann M, Escriou N, Grywna K, Kramme S, Manuguerra JC, Müller S et al (2003) Identification of a novel coronavirus in patients with severe acute respiratory syndrome. N Engl J Med 348:1967–1976. https://doi.org/10.1056/NEJMoa030747
4. Zaki AM, van Boheemen S, Bestebroer TM, Osterhaus ADME, Fouchier RAM (2012) Isolation of a novel coronavirus from a man with pneumonia in Saudi Arabia. N Engl J Med 367:1814–1820. https://doi.org/10.1056/NEJMoa1211721
5. Ou X, Liu Y, Lei X, Li P, Mi D, Ren L, Guo L, Guo R, Chen T, Hu J, Xiang Z, Mu Z, Chen X, Chen J, Hu K, Jin Q, Wang J, Qian Z (2020) Characterization of spike glycoprotein of SARS-CoV-2 on virus entry and its immune cross-reactivity with SARS-CoV. Nat Commun 11:1620. https://doi.org/10.1038/s41467-020-15562-9
6. Vishwanathan, all you need to know about Corona Virus in India (2020). https://www.unicef.org/india/coronavirus/covid-19, UNICEF India
7. Hoehl S, Rabenau H, Berger A, Kortenbusch M, Cinatl J, Bojkova D, Behrens P, Böddinghaus B, Götsch U, Naujoks F, Neumann P, Schork J, Tiarks-Jungk P, Walczok A, Eickmann M, Vehreschild MJGT, Kann G, Wolf T, Gottschalk R, Ciesek S (2020) Evidence of SARS-CoV-2 infection in returning travelers from Wuhan, China. N Engl J Med 382:1278–1280

8. Yu P, Zhu J, Zhang Z, Han Y (2020) A familial cluster of infection associated with the 2019 novel coronavirus indicating possible person-to-person transmission during the incubation period. J Infect Dis 221:1757–1761. https://doi.org/10.1093/infdis/jiaa077
9. Baig A M and Erin C S (2020) Potential Neuroinvasive Pathways of SARS-CoV-2: Deciphering the spectrum of neurological deficit seen in coronavirus disease-2019 (COVID-19). Journal of medical virology 92:1845–1857. https://doi.org/10.1002/jmv.26105, 2020
10. Murugan D, Bhatia H, Sai VVR, Satija J (2020) P-FAB: a Fiber-optic biosensor device for rapid detection of COVID-19. Transactions of the Indian National Academy of Engineering 5: 211–215. https://doi.org/10.1007/s41403-020-00122-w
11. E. Preparedness, Emergency Preparedness and Response CDC Emergency Operations Center Activations. https://emergency.cdc.gov/recentincidents/index.asp, (2020) 2018–2019
12. Quest Diagnostics laboratories in San Juan Capistrano CA, Chantilly VA and Marlboro MA, or other laboratories, (2019). https://www.fda.gov/media/136231/download
13. Chu DKW, Pan Y, Cheng SMS, Hui KPY, Krishnan P, Liu Y, Ng DYM, Wan CKC, Yang P, Wang Q, Peiris M, Poon LLM (2020) Molecular diagnosis of a novel coronavirus (2019-nCoV) causing an outbreak of pneumonia. Clin Chem 66:549–555. https://doi.org/10.1093/clinchem/hvaa029
14. Asif M, Ajmal M, Ashraf G, Muhammad N, Aziz A, Iftikhar T, Wang J, Liu H (2020) The role of biosensors in coronavirus disease-2019 outbreak. Current Opinion in Electrochemistry 23: 174–184. https://doi.org/10.1016/j.coelec.2020.08.011
15. C.-E. Igg, A. Test, Accelerated Emergency Use Authorization (Eua) Summary Covid-19 Elisa Igg Antibody Test (Mount Sinai Laboratory), (2013) 51–58. https://www.fda.gov/media/137029/download
16. COVID research: a year of scientific milestones, Nature. (2021) 41586. https://doi.org/10.1038/d41586-020-00502-w
17. Smart Detect SARS-CoV-2 rRT-PCR Kit Instructions for Use for Emergency Use Authorization (EUA), pp. 1–18, https://www.fda.gov/media/136786/download
18. Lee CS, Kyu Kim S, Kim M (2009) Ion-sensitive field-effect transistor for biological sensing. Sensors 9:7111–7131. https://doi.org/10.3390/s90907111
19. Moon D-I, Han J-W, Meyyappan M (2016) Comparative study of field effect transistor based biosensors. IEEE Trans Nanotechnol 15:956–961. https://doi.org/10.1109/TNANO.2016.2615855
20. Kalra S, Kumar MJ, Dhawan A (2020) Reconfigurable FET biosensor for a wide detection range and electrostatically tunable sensing response. IEEE Sensors J 20:2261–2269. https://doi.org/10.1109/JSEN.2019.2952333
21. Vu CA, Chen WY (2019) Field-effect transistor biosensors for biomedical applications: recent advances and future prospects. Sensors (Switzerland) 19. https://doi.org/10.3390/s19194214
22. Sadighbayan D, Hasanzadeh M, Ghafar-Zadeh E (2020) Biosensing based on field-effect transistors (FET): recent progress and challenges. TrAC Trends Anal Chem 133:116067. https://doi.org/10.1016/j.trac.2020.116067
23. Mukhopadhyay S, Sen D, Goswami B, Sarkar S (2020) Performance evaluation of dielectrically modulated extended gate single cavity InGaAs/Si HTFET based label-free biosensor considering non-ideal issues. IEEE Sensors Journal PP. https://doi.org/10.1109/JSEN.2020.3033576
24. Kanungo S, Rahaman H, Chattopadhyay S (2015) Investigating the performance of short gate insulator less dielectrically modulated tunnel field effect transistor based bio-sensors. In: 2015 6th international conference on computers and devices for communication (CODEC). Pp 1–4. https://doi.org/10.1109/CODEC.2015.7893189
25. Paliwal A, Tomar M, Gupta V (2014) Complex dielectric constant of various biomolecules as a function of wavelength using surface plasmon resonance. J Appl Phys 116:23109. https://doi.org/10.1063/1.4890027
26. Chan M, Assaderaghi F, Hu C et al (1994) Recessed-Channel structure for fabricating ultrathin SOI MOSFET with low series resistance. IEEE Electron Device Letters 15:22–24. https://doi.org/10.1109/55.289474
27. Koh YH, Choi JH, Nam MH, Yang JW (1997) Body-contacted SOI MOSFET structure with fully bulk CMOS compatible layout and process. IEEE Electron Device Letters 18:102–104. https://doi.org/10.1109/55.556094
28. Colinge JP, Chen J, Flandre D, et al (1996) A low-voltage, low-power microwave SOI MOSFET. In: 1996 IEEE international SOI conference proceedings. Pp 128–129
29. Abdullah, M.M., Rajab, F.M., & Al-Abbas, S.M. (2014) Structural and optical characterization of Cr_2O_3 nanostructures: evaluation of its dielectric properties. AIP Adv, 4:*0*–11. https://doi.org/10.1063/1.4867012
30. Kim C, Jung C, Park HG, Choi Y (2008) Novel dielectric-modulated field-effect transistor for label-free DNA detection. Biochip Journal 2:127–134
31. Singh D, Patil GC (2020) Performance analysis of feedback field-effect transistor-based biosensor. IEEE Sensors J 20:13269–13276. https://doi.org/10.1109/JSEN.2020.3006986
32. Parihar MS, Kranti A (2015) Enhanced sensitivity of double gate junctionless transistor architecture for biosensing applications. Nanotechnology 26:145201. https://doi.org/10.1088/0957-4484/26/14/145201
33. Talley K, Ng C, Shoppell M, Kundrotas P, Alexov E (2008) On the electrostatic component of protein-protein binding free energy. PMC Biophys 1:2. https://doi.org/10.1186/1757-5036-1-2
34. Huang Y, Yang C, Xu X feng, et al (2020) Structural and functional properties of SARS-CoV-2 spike protein: potential antivirus drug development for COVID-19. Acta Pharmacol Sin 41:1141–1149. https://doi.org/10.1038/s41401-020-0485-4
35. Igor P, Pushkar R, Tsu-Jae K, Hu C, (2004) Dual work function CMOS gate technology based on metal interdiffusion, U.S. patent, no. US 2004O238859A1,
36. Im H, Huang XJ, Gu B, Choi YK (2007) A dielectric-modulated field-effect transistor for biosensing. Nat Nanotechnol 2:430–434. https://doi.org/10.1038/nnano.2007.180
37. Yadav S, Gedam A, Tirkey S (2021) A dielectric modulated biosensor for SARS-CoV-2. IEEE Sensors J 21:14483–14490. https://doi.org/10.1109/JSEN.2020.3019036
38. ATLAS user's manual, SILVACO Int, Santa Clara, CA (2014)